

Optimizing direct laser-driven electron acceleration and energy gain at ELI-NP

Etele Molnár,¹ Dan Stutman,¹ and Catalin Ticos¹

¹*Extreme Light Infrastructure Nuclear Physics ELI-NP,
Horia Hulubei National Institute for Physics and Nuclear Engineering,
30 Reactorului Street, RO-077125, Bucharest-Magurele, Romania*

(Dated: September 28, 2020)

We study and discuss electron acceleration in vacuum interacting with fundamental Gaussian pulses using specific parameters relevant for the multi-PW femtosecond lasers at ELI-NP. Taking into account the characteristic properties of both linearly and circularly polarized Gaussian beams near focus we have calculated the optimal values of beam waist leading to the most energetic electrons for given laser power. The optimal beam waist at full width at half maximum correspond to few tens of wavelengths, $\Delta w_0 = \{13, 23, 41\} \lambda_0$, for increasing laser power $P_0 = \{0.1, 1, 10\}$ PW. Using these optimal values we found an average energy gain of a few MeV and highest-energy electrons of about 160 MeV in full-pulse interactions and in the GeV range in case of half-pulse interaction.

I. INTRODUCTION

Laser-matter interaction by ultra-intense and ultra-short lasers at the Extreme Light Infrastructure (ELI) are intended to provide new horizons and breakthroughs in technological advancements and fundamental physics.

Laser-driven charge acceleration has been proposed and investigated both theoretically and experimentally during the last few decades [1–6]. Plasma based accelerators are an established method to provide electron beams to GeV energies in short pulse laser wakefield interactions [7, 8]. Compared to different plasma based acceleration mechanisms where the electrons gain energy from the longitudinal fields of charge-separated plasma electrons and ions, i.e., bubble or ion channel [9–14], simple vacuum-based acceleration, or direct laser acceleration (DLA), has been little studied recently. However, vacuum-based acceleration is not only much more straightforward and simpler involving a well defined and understood physical process, but in some cases of interest it might be even favorable due to absence of the plasma.

In this paper, we aim to study and review the characteristics of electron acceleration and ponderomotive scattering in vacuum by femtosecond laser pulses of highest intensity achievable today. In particular, we are interested in determining the dependence of the net kinetic energy gain in the fundamental Gaussian mode, on various laser parameters such as intensity, beam waist, pulse duration and polarization. Our primary purpose is not strictly academic, but we aim to estimate and explore the relevant parameters for laser-driven electron acceleration for the future experiments at ELI-NP [15].

DLA with femtosecond laser pulses and intensities above 10^{19} W/cm², were reported to lead to electrons with kinetic energy of a few MeV [16, 17]. Similarly, here we will study the energy gain of electrons in lasers of intensity, above 10^{22} W/cm², operating at ELI-NP. A possible application of direct electron acceleration is to measure the peak laser intensity in the focal region [18].

Due to the fact that this basic problem in electrodynamics has no known general solution, the interaction of

free electrons with laser fields in vacuum is based on a 3-dimensional numerical code that solves the relativistic equations of motion. In addition to a large number of theoretical papers, e.g., Refs. [19–37], available in the literature, the novelty in our investigation of direct laser acceleration of electrons gives us a good number of valuable estimates and insight specifically for the lasers operating at ELI-NP.

The paper is structured as follows. For the sake of completeness in Sect. II A we recall the relativistic equations of motion of charges in electromagnetic fields. Next we give a brief summary on the fundamental Gaussian beam IIB in the paraxial approximation. The list of parameters and initial conditions corresponding to our study of direct electron acceleration are given in Sect. II C. Our results and discussions are presented in Sect. III. Taking into account the characteristic properties of Gaussian beams we have calculated the optimal values of beam waist leading to the most energetic electrons for given laser power. Using these values we present and discuss the corresponding electron dynamics and energy gains in linearly polarized (LP) and circularly polarized (CP) laser beams. We found an average energy gain of a few MeV where the highest energy electrons are about 160 MeV, in full-pulse interactions. Furthermore in case of half-pulse interaction these energy gains are almost an order of magnitude higher, reaching 1 GeV in agreement with the ponderomotive limit. Finally, the conclusions are summarized in Sect. IV.

II. DIRECT LASER ACCELERATION

A. Charge acceleration in vacuum

Here we briefly review the relativistic equations of motion of a charge q in electromagnetic fields [38]. The contravariant particle four-momentum p^μ is defined as

$$p^\mu \equiv (p^0, \vec{p}) = m_q \gamma c (1, \vec{\beta}), \quad (1)$$

where $m_q = \sqrt{p^\mu p_\mu}/c^2$ is the rest mass of the charged particle, $\vec{p}/p^0 = \vec{v}/c \equiv \vec{\beta}$ is the normalized three-velocity of the particle and $c = 1/\sqrt{\epsilon_0 \mu_0}$ is the speed of light in vacuum. The Lorentz factor is defined as

$$\gamma \equiv \frac{1}{\sqrt{1 - \beta^2}} = \sqrt{1 + \left(\frac{|\vec{p}|}{m_q c}\right)^2}, \quad (2)$$

where $\beta = |\vec{\beta}|$, while the relativistic three-momentum and the energy of the particle are, $\vec{p} = \gamma m_q c \vec{\beta}$ and $p^0 \equiv E^\gamma/c = \gamma m_q c$.

The relativistic equation of motion of charged particles in electromagnetic field is determined by the Lorentz force, $\vec{F}_L \equiv d\vec{p}/dt = q(\vec{E} + \vec{v} \times \vec{B})$. This leads to the following set of coupled ordinary differential equations,

$$\frac{d\vec{x}}{dt} = c\vec{\beta}, \quad (3)$$

$$\frac{d\vec{\beta}}{dt} = \frac{q}{\gamma m_q c} \left[-\vec{\beta}(\vec{\beta} \cdot \vec{E}) + \vec{E} + c\vec{\beta} \times \vec{B} \right], \quad (4)$$

where \vec{x} denotes the position of the particle, while \vec{E} and \vec{B} are the electric and magnetic fields in vacuum. Using the relation from Eq. (2) together with the three independent equations (4), provides and additional equation for the relativistic energy $E^\gamma = \gamma m_q c^2$,

$$\frac{d\gamma}{dt} = \frac{q}{m_q c} (\vec{\beta} \cdot \vec{E}). \quad (5)$$

These equations may be solved in dimensionless form that is found either by setting all fundamental constants to be one, i.e., $|q| = c = m_q = 1$, as chosen by us, or equivalently by introducing new dimensionless variables, i.e., $t_d = t\omega_0$, $\vec{x}_d = \vec{x}\omega_0/c$, $\vec{p}_d = \vec{p}/(m_q c)$, where ω_0 is the angular frequency.

For given initial conditions, the solution of the relativistic Lorentz equations provide the velocities and the 3-dimensional trajectories of a moving charge as function of time. These solutions depend on the electromagnetic field that will be specified in the next section.

B. Gaussian beams

Possibly the most well known particular solution to the paraxial wave equation is the fundamental Gaussian beam [22, 39, 40]. The general expression for the transverse electric field of a Gaussian beam is,

$$E_T(r, z) = E_0 \exp[-ik_0 z + i\phi_0] \times \frac{w_0}{w(z)} \exp\left[-\frac{r^2}{w^2(z)} - i\frac{zr^2}{Z_R w^2(z)} + i \arctan\left(\frac{z}{Z_R}\right)\right], \quad (6)$$

where $k_0 = \omega_0/c$ is the wavenumber, E_0 is the amplitude of the electric field, ϕ_0 is the constant initial phase shift and $r = \sqrt{x^2 + y^2}$ is the radius in the transverse

plane measured from the longitudinal axis of propagation, i.e., z -axis. The radius of curvature is $R_c(z) \equiv (z^2 + Z_R^2)/z = Z_R^2 w^2/(z w_0^2)$, where the Rayleigh range or confocal distance is defined as $Z_R = \frac{w_0^2 k_0}{2}$. Furthermore the Gouy phase at z is given as $\phi_G(z) = \arctan\left(\frac{z}{Z_R}\right)$, while the radius of the Gaussian beam is

$$w(z) = w_0 \sqrt{1 + \left(\frac{z}{Z_R}\right)^2}, \quad (7)$$

where the beam radius at focus (minimum spot size) defines the beam waist radius $w_0 \equiv w(z=0)$. Therefore for a given laser wavelength and polarization the fundamental Gaussian beam has only two parameters, the field intensity and beam waist radius, such that from the latter all other parameters describing the beam geometry are determined. The explicit expressions for the electric field components are,

$$E_x(r, z) = \alpha_x E_T, \quad E_y(r, z) = -i\alpha_y E_T, \quad (8)$$

where $\alpha_x = \sqrt{(1 + \alpha_P)/2}$ and $\alpha_y = \sqrt{(1 - \alpha_P)/2}$ such that $\alpha_P = 1$ or -1 in case of linear polarization along the x -axis or y -axis respectively. Furthermore $\alpha_P = 0$ for circular polarization and elliptic polarization otherwise. Therefore in case of circular polarization the field amplitudes differ by a factor of $1/\sqrt{2}$ from the amplitudes in case of linear polarization.

Assuming harmonic time dependence of the fields $\vec{E} \sim \exp(i\omega_0 t)$, the longitudinal component of the electric field is calculated from $\nabla \cdot \vec{E} = 0$,

$$E_z(r, z) = -\frac{i}{k_0} \left(\frac{\partial E_x}{\partial x} + \frac{\partial E_y}{\partial y} \right). \quad (9)$$

Similarly the components of the magnetic field follow from Maxwell's equations $\vec{B} = \frac{i}{ck_0} \nabla \times \vec{E}$ and $\nabla \cdot \vec{B} = 0$. In the paraxial approximation we have [41]

$$B_x(r, z) = -\frac{1}{c} E_y(r, z), \quad B_y(r, z) = +\frac{1}{c} E_x(r, z), \quad (10)$$

$$B_z(r, z) = \frac{i}{ck_0} \left(\frac{\partial E_y}{\partial x} - \frac{\partial E_x}{\partial y} \right). \quad (11)$$

The finite duration of the pulse is taken into account by assuming the widely used Gaussian temporal envelope [35], where τ_0 is the duration of the pulse and z_F is the initial position of the intensity peak. Therefore introducing,

$$g(t, z) = \exp\left[i\omega_0 t - \left(\frac{t - (z - z_F)/c}{\tau_0}\right)^2\right], \quad (12)$$

the fundamental Gaussian pulse is completely specified by the components of the electric and magnetic fields, Eqs. (8, 9) and Eqs. (10, 11), multiplied by Eq. (12), and finally taking the real part of the expressions,

$$\vec{E}(t, r, z) = \text{Re} \left[\vec{E}(r, z) g(t, z) \right], \quad (13)$$

$$\vec{B}(t, r, z) = \text{Re} \left[\vec{B}(r, z) g(t, z) \right]. \quad (14)$$

C. Initial conditions

In this paper we study direct laser acceleration of a flat electron cloud interacting with different Gaussian pulses. Unless stated otherwise, in the following cases of interest, all electrons are initially at rest, i.e., $\vec{\beta}_{0,i} = \vec{0}$ hence $\gamma_{0,i} = 1$, as well as all initial constant phases are set to zero, i.e., $\phi_{0,i} = 0$. The electron charge will be denoted as, $q = -e$, while its rest mass as $m_e = 0.511 \text{ MeV}/c^2$.

Furthermore all electrons are initially located at $z_i(t_0) \equiv z_{0,i} = 0$ on the optical axis and distributed uniformly in the transverse plane on a 2-dimensional disk with radius that is twice the beam waist radius, i.e., $r_0 = 2w_0$. This guarantees that over 99.9% of the laser energy is contained within this disk. The electron cloud is made of $N = 4000$ randomly distributed non-interacting electrons in the transverse plane for current purposes. Note that in all cases, we have used the same seed for the pseudo-random number generator, hence the initial distribution scales with the radius of the disk.

The laser pulse duration and spot size are specified by values given at Full Width at Half Maximum (FWHM). Therefore a Gaussian of the form, $\exp(-r^2/\sigma^2)$, like in Eqs. (6) and (12), and hence a laser pulse of $\Delta\tau_0$ duration and beam waist of Δw_0 specified at FWHM translates as,

$$\tau_0 = \frac{\Delta\tau_0}{2\sqrt{\ln 2}}, \quad w_0 = \frac{\Delta w_0}{2\sqrt{\ln 2}}. \quad (15)$$

Introducing the normalized electric field amplitude $a_0 = \frac{eE_0}{m_e c \omega_0}$, the peak intensity for a linearly polarized Gaussian beam is

$$I_0 \equiv E_0^2 \frac{c\epsilon_0}{2} = a_0^2 \left(\frac{m_e c \omega_0}{e} \right)^2 \frac{c\epsilon_0}{2} = 3.856 \times 10^{-9} a_0^2 \omega_0^2. \quad (16)$$

The total power carried by the laser beam is $P_0 \equiv I_0 \frac{\pi w_0^2}{2} = 6.057 \times 10^{-9} a_0^2 w_0^2 \omega_0^2$ and hence the value of a_0 for a given power and initial waist radius w_0 is obtained from

$$a_0 \equiv 1.285 \times 10^4 \frac{\sqrt{P_0}}{w_0 \omega_0} = 1.61 \times 10^4 \frac{\sqrt{I_0}}{\omega_0}. \quad (17)$$

The value of a_0 defined above corresponds to a LP laser $a_{0,LP} = a_0$, while in case of a CP laser we have $a_{0,CP} = \frac{1}{\sqrt{2}} a_0$. Thus for a monochromatic laser with wavelength $\lambda_0 = 800 \text{ nm}$, for any given laser power and waist radius w_0 , the normalized field intensities a_0 are determined from Eq. (17).

For our cases of interest choosing, $\Delta w_0 = 13\lambda_0$, $\Delta w_0 = 23\lambda_0$ and $\Delta w_0 = 41\lambda_0$, the corresponding peak intensity values are listed for a linearly polarized Gaussian pulse in Table I. The outcome of these different cases will be discussed in the next sections.

III. RESULTS FOR THE FUNDAMENTAL GAUSSIAN BEAM

Here we present and discuss in detail the 3-dimensional numerical solutions to particle trajectories and velocities and the space-time evolution of the laser pulse. These solutions are obtained by solving the equations of motion Eqs. (3, 4) together with the electromagnetic field of the propagating laser pulse Eqs. (13, 14) for a large number of independent and randomly distributed electrons. The numerical solutions are required to have accuracy and numerical precision up to 12-digits, by using an adaptive time-step Runge-Kutta method available in programming languages like Mathematica or Matlab.

The physics of laser-driven electron acceleration in vacuum follows from the direct interaction of the laser pulse with electrons as given by the Lorentz force, Eqs. (3,4). For $a_0 \geq 1$, the energy and momentum oscillations induced by the laser become relativistic, and the Lorentz force converts a large part of the laser's energy into longitudinal momentum.

Any electric charge interacting with the laser pulse is accelerated by the electric and magnetic fields therein. Therefore a point-like charge gains momentum and will get displaced from its current location to a new position, where the electric and magnetic fields of the laser pulse are in general different from before (one time-step earlier). In this way, the propagating electric charge dynamically maps the laser pulse's electric and magnetic fields along its trajectory. To explain it in another way, since the electromagnetic field is function of both space and time, therefore at any given time the particle trajectories, i.e., the solutions to Eqs. (3,4), serve as input, space-time coordinates, for the electromagnetic field of the pulse, i.e., Eqs. (13, 14).

Furthermore, the electric field, Eqs. (8), and thus the intensity of the Gaussian pulse is highest at the center $x_0 = y_0 = z_0 \equiv 0$, i.e., peak intensity, but decreases exponentially with increasing transverse radial distance r^2 . Since the charges are distributed randomly in the transverse plane the available electric and magnetic fields are also different in different positions. Therefore, in general the net energy gain of electrons interacting with a laser pulse is a function of the intensity and a function of the initial position of charges in the focus of the laser and the beam waist. In the next sections, we will discuss these cases in more detail.

A. Full pulse interaction $z_F = -5\tau_0 c$

In this case we assume that the initial position of the peak of the Gaussian laser pulse is located on the optical axis behind the charges at $z_F = -5\tau_0 c$. This guarantees that the electric field in the front part of the pulse initially acting on the electrons is vanishingly small, and therefore the initial constant phases are not affecting the trajectories.

P_0 [PW]	I_0 [W/cm ²]	$w_0 = 7.8\lambda_0$	I_0 [W/cm ²]	$w_0 = 13.8\lambda_0$	I_0 [W/cm ²]	$w_0 = 24.6\lambda_0$
0.1	1.63×10^{20}	$a_0 = 8.73$	5.21×10^{19}	$a_0 = 4.94$	1.64×10^{19}	$a_0 = 2.77$
1	1.63×10^{21}	$a_0 = 27.63$	5.21×10^{20}	$a_0 = 15.62$	1.64×10^{20}	$a_0 = 8.76$
10	1.63×10^{22}	$a_0 = 87.37$	5.21×10^{21}	$a_0 = 49.4$	1.64×10^{21}	$a_0 = 27.7$

TABLE I. The values of peak intensity and normalized field amplitude corresponding to different waist radii and laser powers.

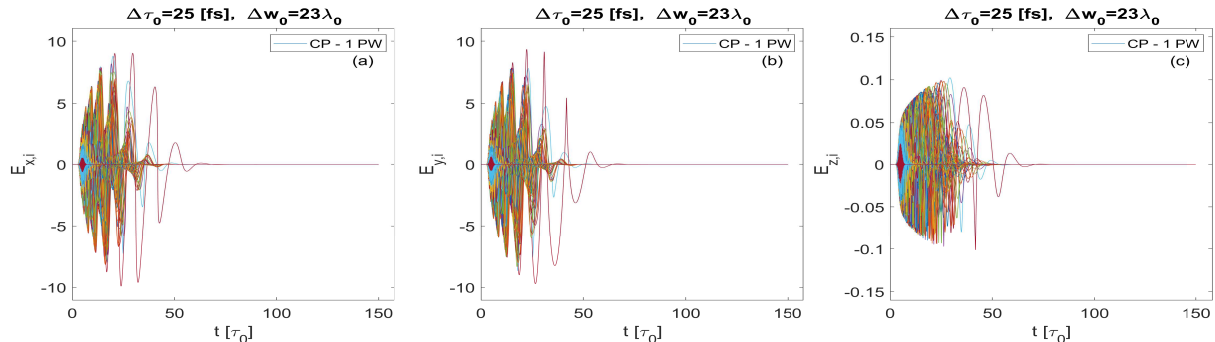


FIG. 1. From left to right in (a), (b) and (c) respectively: The Cartesian components of the electric field, $E_{x,i}$, $E_{y,i}$, $E_{z,i}$, as seen by the charges in units of the normalized field intensity a_0 , as a function of time normalized by the pulse duration. The parameters of the Gaussian laser pulse are shown on the figure.

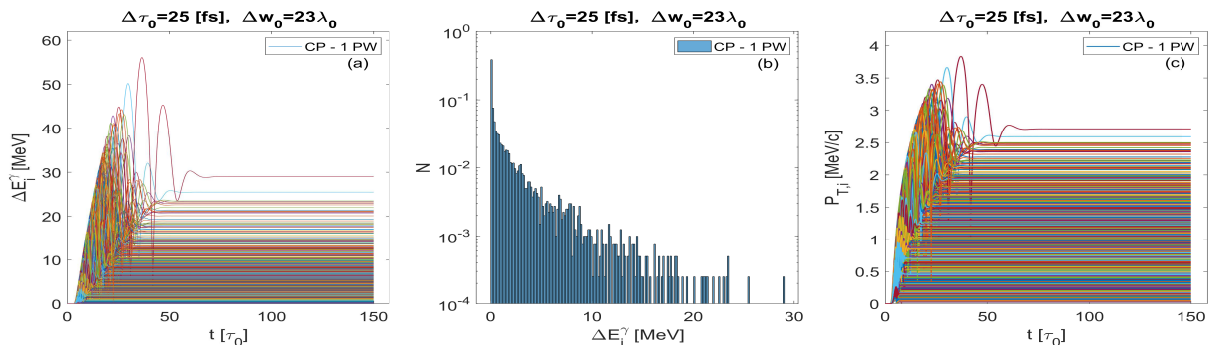


FIG. 2. From left to right: (a) The net energy gain of electrons, ΔE_i^γ , as a function of time, and the corresponding histogram (b), followed by the transverse momentum $P_{T,i}$ of electrons (c). The parameters of the laser pulse are shown on the figure.

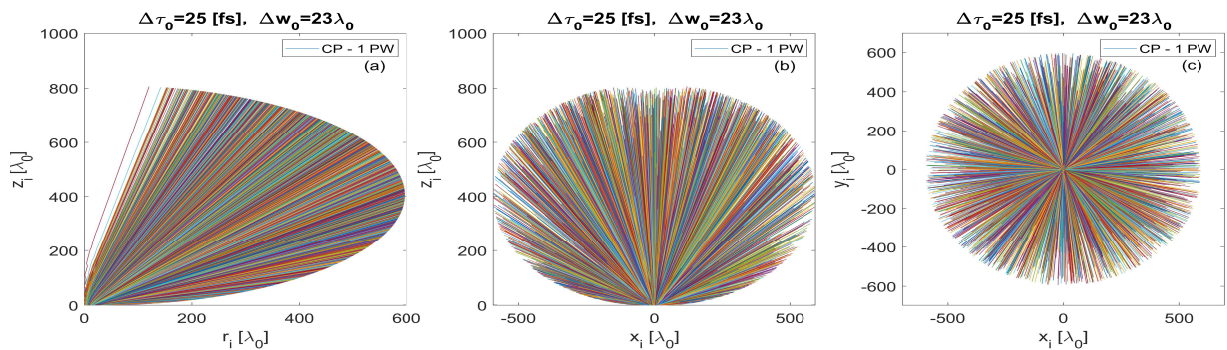


FIG. 3. From left to right: (a) and (b) The longitudinal trajectories z_i , as function of the radial distance r_i , and as a function of x_i . (c) The electron trajectories in the transverse plane (x_i, y_i) . The parameters of the laser pulse are shown on the figure.

A circularly polarized $P_0 = 1$ PW Gaussian beam of $\Delta\tau_0 = 25$ fs pulse duration and focal spot diameter of $\Delta w_0 = 23\lambda_0$ at FWHM, was shot on a flat disk of electrons, according to the initial conditions summarized in Sect. II C. Since the laser pulse is initially behind the

particles, the electrons are only gradually overtaken and accelerated by the propagating pulse. In Fig. 1 we have plotted the Cartesian components of the electric field seen by the electrons with lower i -index as a function of time. The longitudinal component of the electric field

$E_{z,i}$ was calculated from Eq. (9) leading to almost 2-orders of magnitude smaller values than the corresponding transverse components of the electric field [42]. In a linearly polarized pulse these longitudinal field components will decelerate the electron and reduce the net-energy gain [22, 25]. However in a circularly polarized Gaussian pulse the effect is opposite and the electrons are accelerated by the longitudinal fields.

The visible asymmetry in the time-evolution of the electric field as traced by the particles, is partially caused by the longitudinal components of the $\vec{v} \times \vec{B}$ force and of the electric field, as well as by the temporal envelope of the finite pulse. The electrons are accelerated to larger and larger velocities in the front part of the pulse and thus the electron trajectories will become elongated in the direction of the laser propagation. Therefore the deceleration in the back part of the pulse becomes less efficient, hence the asymmetry.

Also note that the normalized electric field amplitudes corresponding to the peak pulse position have intensities that are larger (see the a_0 values in Table I) than accessible to even the highest energy electrons during the interaction with the pulse. This means that the electrons were scattered out of the pulse earlier and without reaching the available peak intensity of the pulse.

In Fig. 2a the time-evolution of the net energy gain of electrons

$$\Delta E_i^\gamma(t) \equiv E_i^\gamma(t) - E_i^\gamma(t_0) = (\gamma_i - 1) m_e c^2, \quad (18)$$

is shown, where the initial energies are $E_i^\gamma(t_0) = m_e c^2$. The corresponding histogram and the evolution of the electrons transverse momentum $P_{T,i} = \sqrt{p_{x,i}^2 + p_{y,i}^2}$ are also shown in Figs. 2b and 2c. Comparing the gain in energy to the gain in transverse momentum we see that the kinetic energy of particles is predominantly contained in the longitudinal momentum, i.e., $p_z = \gamma m_e v_z$.

Furthermore, we also observe from the energy histogram that about 40% of electrons gain very little or no net energy from the laser pulse. This is due to the fact that the initial transverse area where the electrons are located is relatively large, i.e., $r_0 = 2w_0$, while the intensity of the electromagnetic field falls off exponentially with the transverse radius squared. Therefore for $r_0 \leq 1.1w_0$ more than 90% of the laser power is captured while the electrons beyond this transverse area are interacting with relatively weak fields which results in low energy gains.

The charges initially located around the laser axis, are pushed out from the center by the radial ponderomotive force. The full particle trajectories are shown in Figs. 3a-3c, a long time after the laser pulse passed. In Fig. 3a, we have plotted the longitudinal trajectories as a function of the radial distance from the origin. Similarly, Fig. 3b shows the longitudinal trajectories as function of one of the transverse axes, x -axis. The plot as a function of the other transverse axis is very similar, therefore not shown. Observe that the trajectories in the longitudinal direction are on average twice longer than in the

transverse directions, meaning that the average velocities in the longitudinal direction are also larger than in the transverse directions, as already concluded before.

Furthermore, it is also interesting to note that the particles around the center have all scattered out with a polar angle of $\theta_i = \arccos(z_i/r_i) \geq 0$. For a given waist radius this angle decreases with increasing laser power, meaning that the particles around the center will gain larger longitudinal velocities and travel farther in the longitudinal direction.

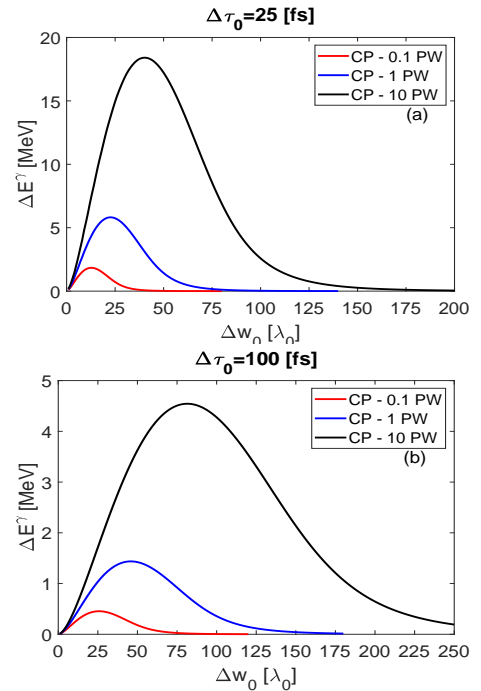


FIG. 4. The average energy gain of an electron initially located at $z_0 = 0$ and $x_0 = y_0 \equiv \{0.1, 0.15, \dots, 1.1\} w_0$ as a function of the beam waist. The red, blue and black lines correspond to the weighted average energy for laser powers of $P_0 = \{0.1, 1, 10\}$ PW respectively. The laser pulse duration is (a) $\Delta \tau_0 = 25$ fs and (b) $\Delta \tau_0 = 100$ fs as shown on the top of the figure. These results are practically independent of the polarization, hence only the CP results are shown.

B. Optimizing the waist of Gaussian pulses

The energy gain of charges interacting with the fundamental Gaussian laser pulse is not a linear function of the initial location of electrons or the beam waist. Here we have estimated the value of the beam waist that correspondingly leads to maximum energy gains. First, for a given laser power and for all discrete values of $\Delta w_0 = \{1, 2, \dots, 250\} \lambda_0$ we have varied the initial position of particles such that they are located at given transverse coordinates $x_0 = y_0 \equiv \{0.1, 0.15, \dots, 1.1\} w_0$, and then calculated the respective energy gains. Then for every given laser power we have calculated the radially weighted average of these results, i.e., $\Delta E_r^\gamma =$

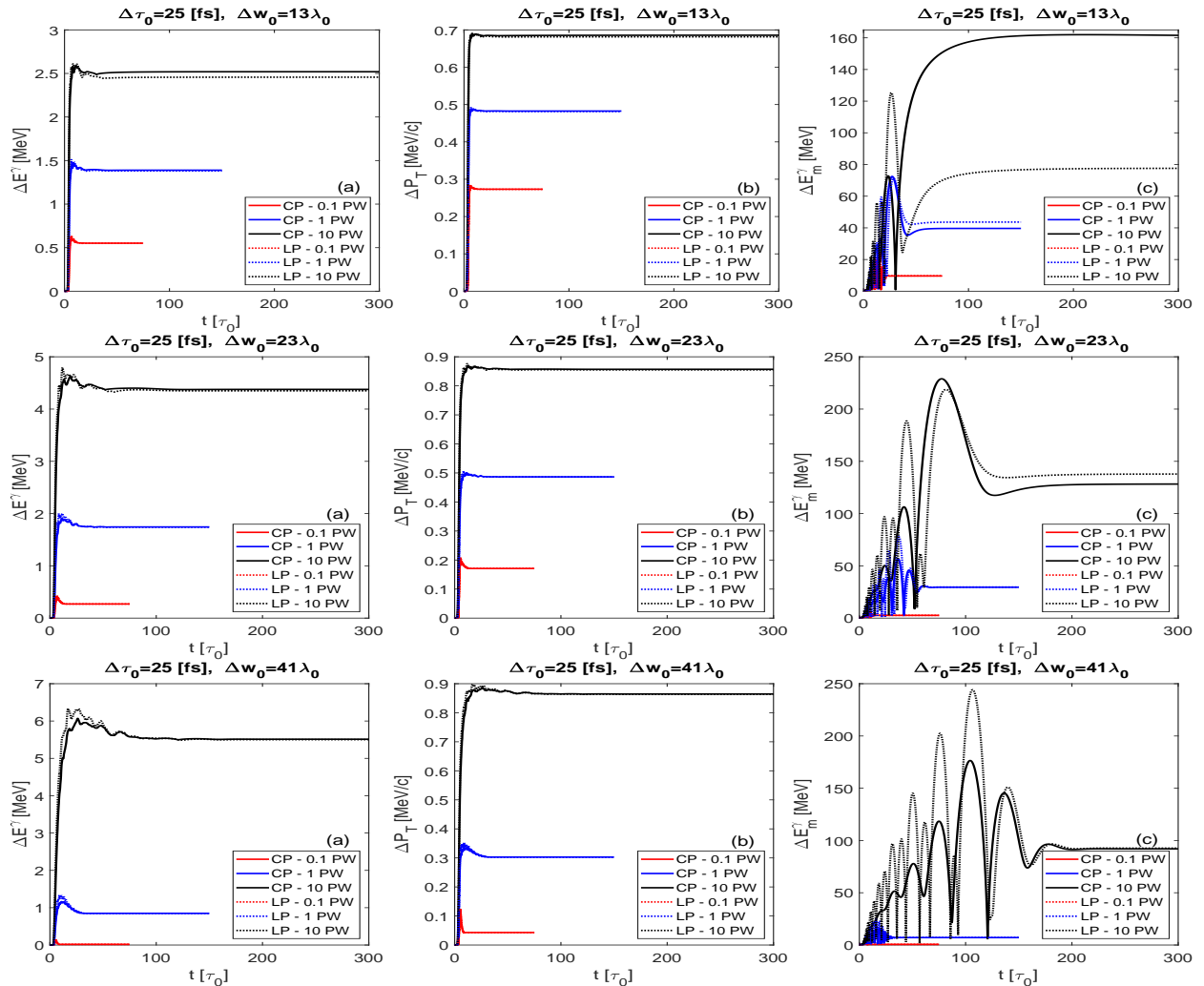


FIG. 5. Upper row: All figures correspond to $\Delta w_0 = 13\lambda_0$ beam waist. From left to right: (a), (b) and (c) respectively. The time evolution of the mean net energy gain of electrons for laser powers of $P_0 = \{0.1, 1, 10\}$ PW, with red, blue and black correspondingly. The full and dotted lines are for circularly and linearly polarized pulses respectively. Similarly, (b) shows the average transverse momentum gained from the pulse as a function of time. The rightmost figure (c), shows the time evolution of the highest energy electron, ΔE_m^γ , corresponding to given laser power. Middle row: The same as the before, but for an initial beam waist of $\Delta w_0 = 23\lambda_0$. Lower row: The same as the before, but for an initial beam waist of $\Delta w_0 = 41\lambda_0$.

$\sum_i r_i \Delta E_i^\gamma / \sum_i r_i$. These weighted averages are shown in Fig. 4a and Fig. 4b for different pulse durations and laser powers. Henceforth for given laser power, we can read the values of beam waist corresponding to the peak in energy gain. For a laser with $\Delta\tau_0 = 25$ fs, these values are also listed in Table I, and hence represent the optimal values for direct electron acceleration for given laser power at ELI-NP.

Increasing the laser power will increase the net energy gain for a given spot size, see Figs. 4 which allows the comparison of the energy gain at any given waist. At the same time, for any given laser power, increasing the beam waist also leads to an increase in the energy gain. This is because for a wider beam waist, the scattering of the electrons decreases and hence they may remain confined in the pulse for longer. As a consequence they are able to extract more energy and momentum from the laser.

With increasing intensity the amplitude of the electron oscillations along the polarization direction increases until it becomes larger than the size of the beam, and the electrons scatter out in the transverse direction.

On the other hand, increasing the beam waist leads to an increase in energy gain at first, but only until the net energy gain reaches a peak or saturation point which corresponds to the optimal beam waist for given laser power. Increasing the waist radius any further than the corresponding peak value will in fact, lead to a decrease in net energy exchange with the laser. This is because, widening the beam waist beyond optimal values will reduce the longitudinal components of the electromagnetic forces. Thus in conclusion for larger laser power a wider but optimal initial waist ensures that the electrons remain confined inside the pulse for longer and hence accelerated to higher energies.

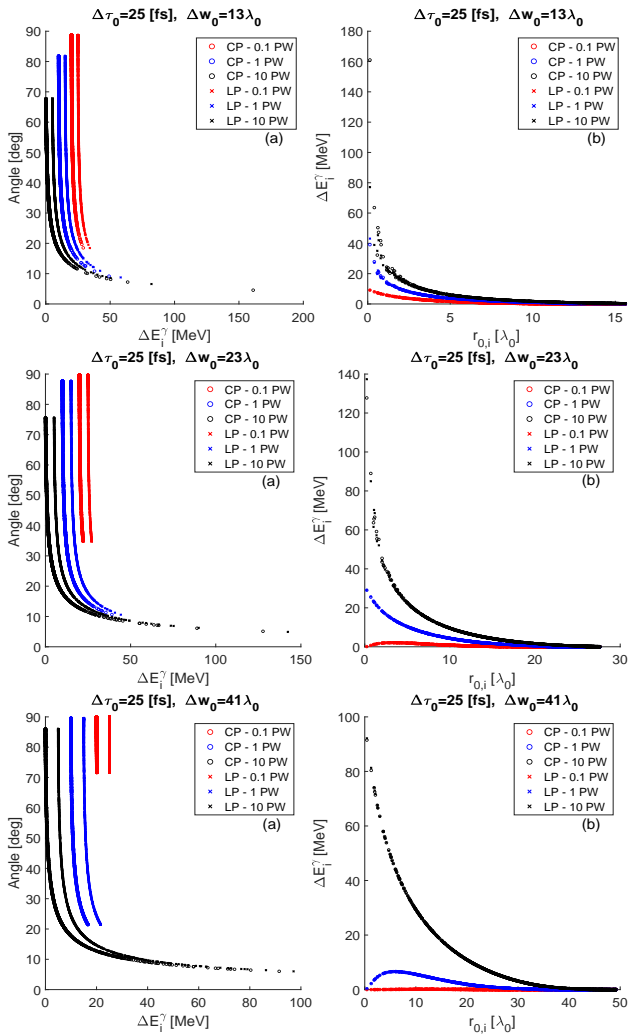


FIG. 6. From left to right (a) and (b): The figure on the left shows the scattering angle calculated from Eq. (19) as a function of energy gain. The data points corresponding to the CP and LP pulse are plotted with "o" and "x". For better visibility, otherwise the data points they lay on the same curve, the data corresponding to a CP pulse with 0.1 PW and 1 PW, red and blue, are shifted by 10 and 20 MeV. Similarly for the LP pulses the points are shifted to the right by 5, 15, 25 MeV. (b) The figure on the right shows the energy gained from the pulse as a function of the initial radial distribution of electrons. The CP and LP results are basically indistinguishable. Middle row: The same as before, but for an initial beam waist of $\Delta w_0 = 23\lambda$. Lower row: The same as before, but for an initial beam waist of $\Delta w_0 = 41\lambda$.

How much energy and momentum the electrons gain also depends on the duration of the laser pulse. For any given laser power increasing the pulse duration decreases the energy gain, as it should be since for a given power, $P_0 \sim \Delta E^\gamma / \Delta t$. Therefore for optimal energy gain, a longer pulse requires longer time spent inside the pulse, which translates to a wider beam waist. Reading and comparing the data from Figs. 4, for a given laser power increasing the pulse duration by a factor of four, requires

approximately two times larger beam waist radius.

Now, using the optimal values for the beam waist at given laser power, we have studied the electron dynamics for laser pulses of $\Delta\tau_0 = 25$ fs duration corresponding to the nine different cases listed in Table I. These are shown in Figs. 5 for circularly and linearly polarized pulses.

The rightmost columns of Figs. 5 show the time evolution of the average energy gained corresponding to different waist sizes. The energy averages $\Delta E^\gamma = \frac{1}{N} \sum_{i=1}^N \Delta E_i^\gamma$ for $N = 4000$ electrons from circularly polarized with full lines and from linearly polarized Gaussian pulses with dotted lines are shown in Figs. 5a. Similarly, Figs. 5b show the average transverse momentum, $\Delta P_T = \frac{1}{N} \sum_{i=1}^N \sqrt{p_{x,i}^2 + p_{y,i}^2}$, while the leftmost columns in Figs. 5c show the electrons with the highest energy gain, ΔE_m^γ , at given waist size and laser power.

The right columns of Figs. 6 show the net energy gain as a function of the initial transverse radial distance, $r_{0,i} \equiv r_i(t_0) = \sqrt{x_{0,i}^2 + y_{0,i}^2}$, from the origin at $z_{i,0} \equiv z_i(t_0) = 0$ for varying laser power. Furthermore, from the conservation of energy and momentum it follows that, the electrons that were initially at rest are ejected out from the pulse with an angle of [6, 20, 25],

$$\theta_i^\gamma = \arctan \left(\sqrt{\frac{2m_e c^2}{\Delta E_i^\gamma}} \right). \quad (19)$$

This so-called ponderomotive scattering angle as a function of energy gain is represented by black, blue, and red symbols for given laser power in Figs. 6b. For example comparing the red data points for the different waist sizes, we see that for a given laser power the scattering angles reach the smallest values for the optimal beam waist. Similarly for the highest laser power the scattering angle asymptotically decreases as a function of energy. These curves are insensitive to the polarization plotted with "o" and "x" for CP and LP beams, hence for better visibility the blue and red data points are shifted by 10, 20 MeV in the CP case compared to the black "o" symbols touching the vertical axis. Similarly in the LP case the black, blue, and red, "x" symbols are shifted by 5, 15, 25 MeV.

As previously discussed, the intensity of Gaussian beam falls off exponentially as a function of the radius squared, hence the charges found further away from the center will gradually gain less and less energy. This is so because the laser intensity and hence the radial ponderomotive decreases with the increase of beam waist and the charges remain confined near the center. However, for larger radial distance from the center, the energy gain increases, up to a maximum, while further away the electrons will gain less energy attributed to the shorter time/length span in the pulse, see the blue and red data points in the lower row of Fig. 6b. Therefore the lower energy electrons are more likely to scatter out with larger θ^γ angles as shown in Figs. 6a.

The overall conclusions regarding the energy gain in full Gaussian pulse interactions are straightforward. The

average energy gain of electrons increases with increasing laser power, and for a given laser power it is largest for an optimal beam waist Δw_0 . For example comparing the black lines in the first column of Figs. 5, corresponding to $P_0 = 10$ PW power, we see that for the highest laser power, the largest mean energy is gained for the largest beam waist. Similarly comparing the red lines corresponding to the lowest power laser, i.e., $P_0 = 0.1$ PW, the smallest beam waist leads to the largest average energy gains, as expected.

Furthermore, in the case of the smallest waist size, i.e., $\Delta w_0 = 13\lambda_0$, increasing the power of the laser by two orders of magnitude leads about 5 times increase in net average energy gain, i.e., $\Delta E_{10PW}^\gamma \approx 5 \times \Delta E_{0.1PW}^\gamma$. On the other hand if we compare the average energy gained from the $P_0 = 10$ PW laser in case we increase the beam waist about $\sqrt{10}$ times to $\Delta w_0 = 41\lambda_0$, the results change only about a factor of 2, as a function of the waist size, i.e., $\Delta E_{13\lambda_0}^\gamma \approx 2.3 \times \Delta E_{41\lambda_0}^\gamma$. In this case the relatively large waist also leads to a decrease in the energy gain from the less powerful laser, i.e., $P_0 = 0.1$ PW, by more than an order in magnitude.

In all cases, the average energy gain is about a few MeV at most, while the maximum energy gain could be about 20 – 30 times of this average for the highest intensity. For peak intensities above 10^{19} W/cm² corresponding to a 0.1 PW laser, electrons with kinetic energy of a few MeV were reported in Refs. [16, 17], in agreement with our results. For intensities above 10^{21} W/cm², relatively few electrons that are initially found in the close vicinity of the longitudinal axis, where the intensity is largest, the net energy gain may reach $\Delta E^\gamma \simeq 100 - 160$ MeV. This energy gain is comparable to a few times $m_e c^2 a_0$, while for $a_0 \geq 5$ the peak energy gain is $\Delta E^\gamma \geq m_e c^2 a_0$. Note that for the $P_0 = 10$ PW laser, the dimensionless transverse coordinates leading to largest energy are $x_{0,d} = 0.677$ and $y_{0,d} = 0.484$ for $\Delta w_0 = 13\lambda_0$. These values are scaled by 23/13 and 41/13 for the larger spots.

We stress here again, that these results are practically insensitive to the polarization of the laser. For the largest part of the randomly distributed electrons there are no observable differences between the mean or the maximum energy gained due to the polarization of the laser. Of course, the maximum energy gained temporarily during the interaction might be larger in case of linear polarization due to the difference in intensity, field, and electron dynamics but that might not be reflected in the exit energies after scattering.

We also note that around the very center of the Gaussian pulse in the close vicinity of the intensity maximum the differences between CP and LP become visible especially for the smallest beam waist as apparent in Fig. 5c. On the other hand, we have verified that for an already very small radius of $r_0 = 0.15w_0$ that contains about 5% of laser power transmitted at the highest intensity, the differences between the energy gains are only about a few MeV. The larger the radius around the intensity peak the smaller the average intensity while the

differences between CP and LP are diminished. This is clearly reflected even for the highest laser power where for the larger beam waists no difference between CP and LP pulses are observed.

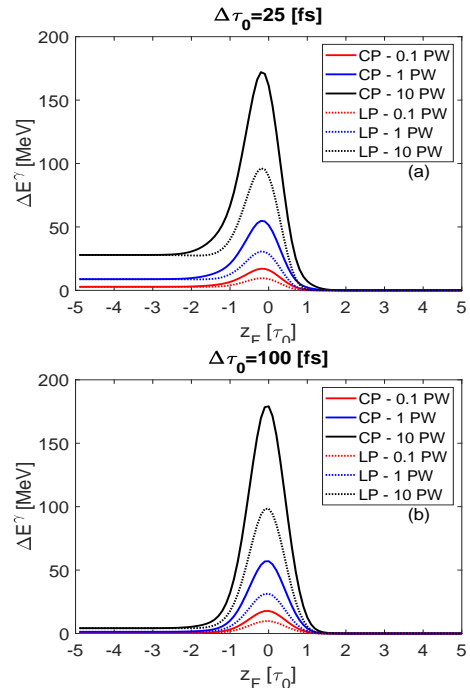


FIG. 7. The energy gain of an electron initially found at $z_0 = 0$ and $x_0 = y_0 \equiv r_0/2$ as a function of the pulse peak position z_F . (a) The figure on the top corresponds to a $\Delta\tau_0 = 25$ fs pulse duration. (b) The figure on the bottom for $\Delta\tau_0 = 100$ fs pulse duration. The red, blue and black dotted and full lines correspond to initial waist radii of $\Delta w_0 = \{13, 23, 41\} \lambda_0$ and laser powers of $P_0 = \{0.1, 1, 10\}$ PW respectively. The dotted lines represent energy gain in linearly while the full lines in circularly polarized Gaussian beams.

C. Partial and half pulse interaction $z_F = 0$

In this section we discuss the effect of shifting the position of the initial intensity peak z_F or the focus of the laser pulse while keeping the electrons at $z_0 = 0$ on the optical axis. The shift of the intensity peak corresponds to changing the interaction domain of the laser pulse [43], and therefore we can investigate the dependence of energy gain on the temporal envelope and the longitudinal position of the focus of the pulse.

It is well known that in a symmetric pulse the energy gained from the front or the first half of pulse is gradually lost in the other half of the pulse throughout the optical cycles. Therefore by gradually removing the first part of the pulse, the electrons will not lose but retain a larger net energy. This is essentially what happens when a prepulse or the front of the pulse reaches and ionizes the matter while leaving behind free electrons at rest. Therefore such electrons are not captured by the whole

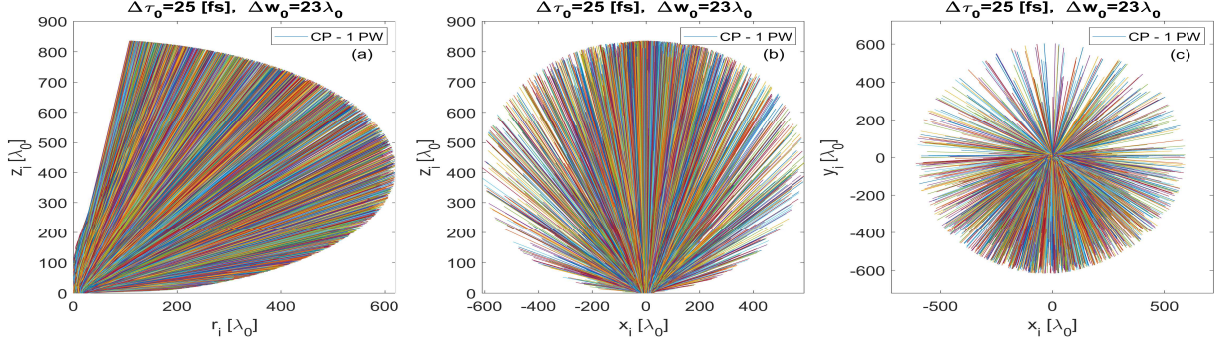


FIG. 8. The same as Fig. 3 but for $z_F = 0$. (a) The electron trajectories in coordinate space. (b) The longitudinal trajectories z_i , as function of the radial distance r_i , and as a function of x_i . (c) The trajectories in the transverse plane (x_i, y_i).

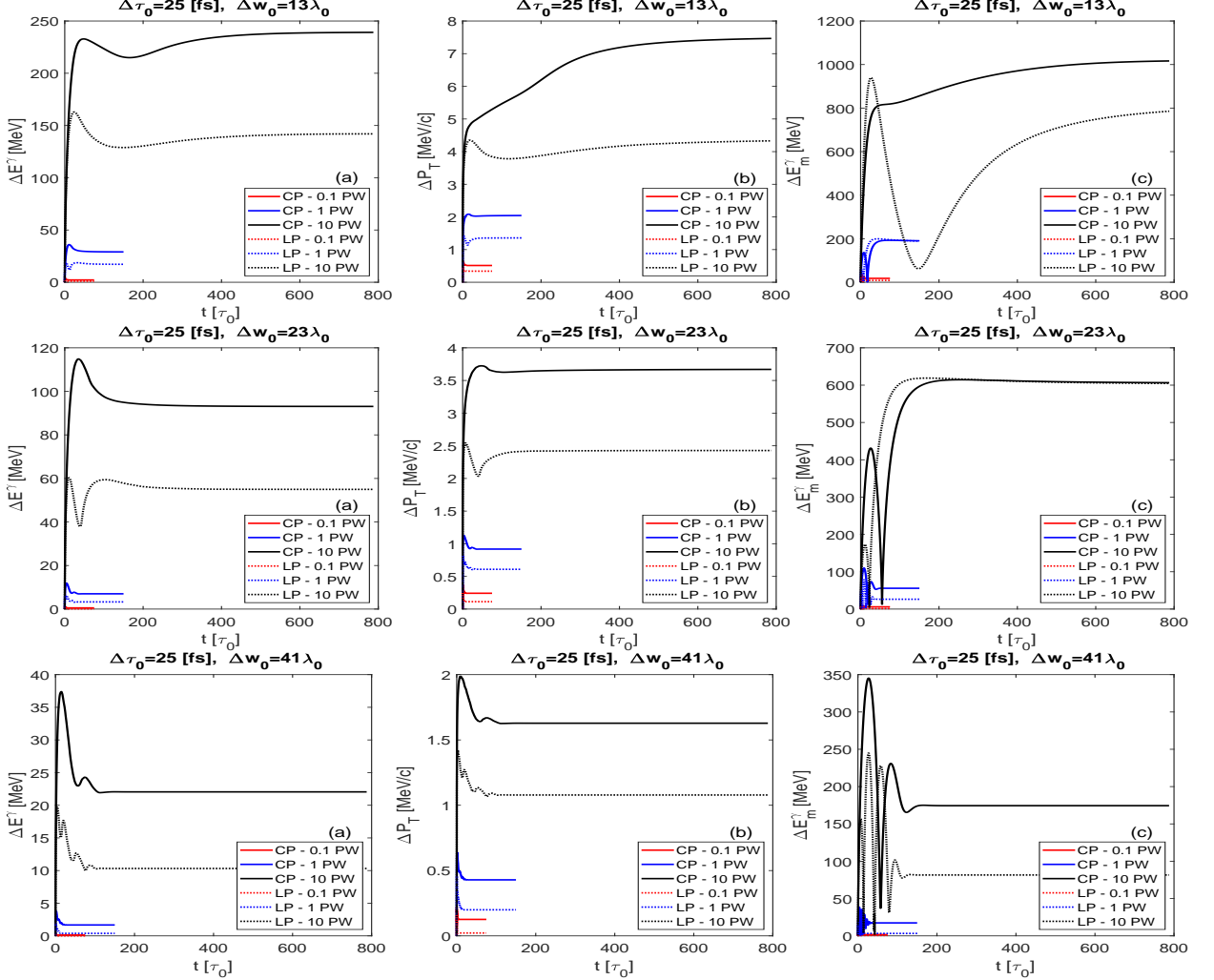


FIG. 9. The same as Fig. 5, except for $z_F = 0$. Upper row: with initial beam waist of $\Delta w_0 = 13\lambda_0$. (a) The time evolution of the mean net energy gain of electrons for laser powers of $P_0 = \{0.1, 1, 10\}$ PW, with red, blue and black correspondingly. The full and dotted lines are for CP and LP pulses respectively. (b) the average transverse momentum gained from the pulse as a function of time. (c) the time evolution of the highest energy electron corresponding to given laser power. Middle row: with initial beam waist of $\Delta w_0 = 23\lambda_0$. Lower row: with initial beam waist of $\Delta w_0 = 41\lambda_0$.

pulse and hence their evolution is different.

For this study, we have kept the optimal parameters as listed in Table I, but now we have fixed the initial position

of electrons at $x_0 = y_0 \equiv w_0/2$. Using this setup, the longitudinal position of the peak of the pulse was varied between $z_F = (-5\tau_0 c, 5\tau_0 c)$, and we have plotted the net

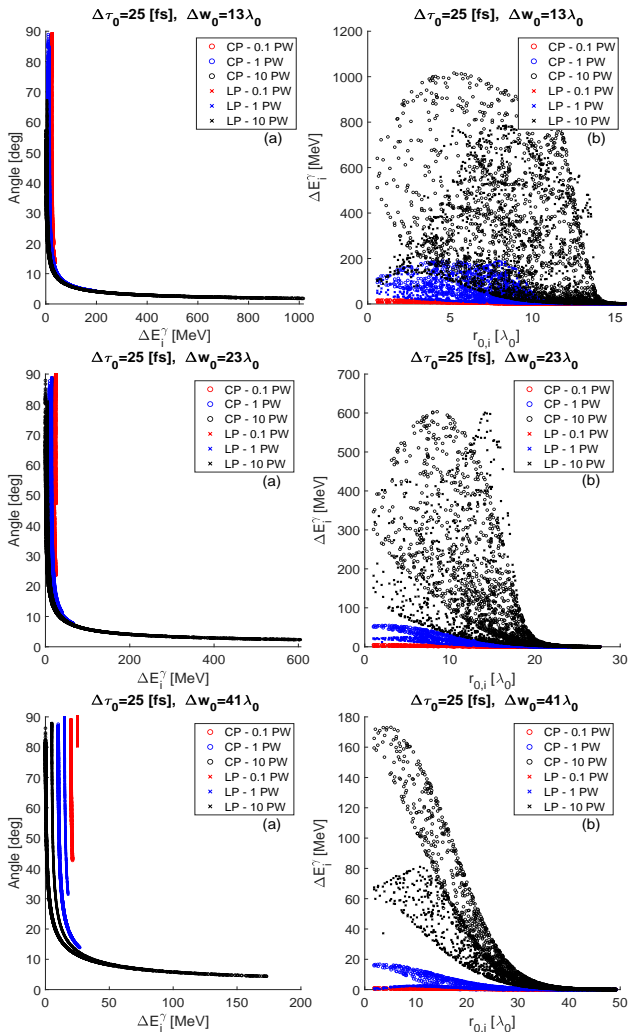


FIG. 10. The same as Fig. 6, except for $z_F = 0$. (a) The scattering angle as a function of energy gain. The data points are shifted for better visibility, otherwise they lay on the same curve. (b) The energy gained from the pulse as a function of the initial radial distribution of electrons. Middle row: with initial beam waist of $\Delta w_0 = 23\lambda$. Lower row: with initial beam waist of $\Delta w_0 = 41\lambda$.

energy gained as a function of z_F .

The outcome of this analysis is shown in Fig. 7 for different laser powers and polarizations. We observe that starting about $z_F > -2\tau_0$ and approaching $z_F \simeq 0$ we obtain larger and larger energy gains. This is due the fact that we are gradually removing the front part of the laser pulse, i.e., we modify the Gaussian time-envelope, see Eq. (12). The temporal envelope, is centered at $z_F = 0$ and decreases with increasing $|z_F|$. Therefore larger initial field amplitudes lead to larger acceleration.

For $z_F \lesssim -2\tau_0 c$, we observe that the energy gain is independent on the polarization, in accordance with our previous results. However, in contrast to the previously studied case already for $z_F > -2\tau_0 c$ the optical polarization of the pulse becomes important. We found that for $z_F \approx 0$ a circularly polarized pulse may lead to almost

two times larger energy gain than a linearly polarized pulse albeit the latter has a larger amplitude.

Similarly to the previous sections III A and III B, here we have analyzed the case of half-pulse interaction using a pulse envelope with $z_F = 0$. With such initial conditions, the particle trajectories and energy gains have changed considerably.

The main difference between full-pulse and half-pulse interaction for circularly polarized Gaussian laser is a strongly anisotropic distribution in both the transverse and longitudinal directions. There are more electrons scattered in the negative than in the positive y -direction, see the particle trajectories shown in Figs. 8b and 8c. This is also true in case of a LP laser, however it is much less pronounced than in the former case.

Now, once again using the different cases listed in Table I, we show and compare the corresponding results in Figs. 9 for circularly and linearly polarized Gaussian beams respectively. The results obtained in case of half pulse interaction lead to the following observations.

The maximum net energy gained (for initially zero constant phases) obtained in half pulse interaction, can be almost an order of magnitude larger, i.e., $\Delta E^\gamma \simeq 1$ GeV, than from full pulse interaction as shown on Figs. 9. This maximum kinetic energy gain is in agreement with the theoretical approximation [23, 27], the so-called ponderomotive limit $\Delta E^\gamma \approx m_e c^2 a_0^2 / 2$, and favors circularly polarized rather than linearly polarized pulses, hence it is best estimated by $a_{0,CP}$ instead of $a_{0,LP}$. We also note here that within or beyond the ponderomotive limit, energy gain of GeV magnitude can also be realized in other various regimes, see Refs. [35, 44, 45]. Note that, in contrast to full-pulse interactions, in half-pulse interactions the initial phase of electrons, i.e., position, is of importance for the energy gain, as shown in Figs. 10b.

In conclusion the net energy gain increases with intensity and decreasing beam waist and the optimal value is given by the smallest waist for a given laser power. Furthermore since the energy gained is also a function of the interaction area covered by the laser pulse, more net energy is retained when the electron interacts with smaller frontal area of the pulse.

IV. CONCLUSIONS

In this paper we have studied direct laser acceleration of electrons by fundamental Gaussian pulses relevant for multi-PW femtosecond lasers at ELI-NP.

In the case of full pulse interactions we have estimated the optimal values of beam waist and we have found that the net energy gain increases with increasing laser power but at the same time it is largest for an optimal beam waist Δw_0 . The optimal beam waists at full width at half maximum correspond to $\Delta w_0 = \{13, 23, 41\} \lambda_0$ for laser powers of $P_0 = \{0.1, 1, 10\}$ PW. In our study we have obtained an average energy gain of a few, i.e., 2–6 MeV and highest-energy electrons about 160 MeV for the 10

PW laser, for these optimal values. On the other hand in the case of half-pulse interaction the average energy gain can be of the order of 100's MeV for the tightest waist of $\Delta w_0 = 13\lambda_0$ with highest energy electrons of 1 GeV for the 10 PW laser.

An investigation of DLA with higher-order Laguerre-Gaussian modes will follow the present work.

ACKNOWLEDGMENTS

The authors thank D. Doria, Z. Harman, K. Spohr, J. F. Ong and K. Tanaka for suggestions and corrections. E. Molnár also thanks H. S. Ghotra for the comparison

of early results and valuable discussions. D. Stutman acknowledges support by a grant of Ministry of Education and Research, CNCS-UEFISCDI, project number PN-IIIP4-ID-PCCF-20160164, within PNCDI III. The authors are thankful for financial support from the Nucleu Project PN 19060105.

AUTHOR CONTRIBUTION STATEMENT

E.M. performed the calculations and the preparation of the manuscript. All the authors have read, supported and approved the final manuscript.

-
- [1] K. Shimoda, *Appl. Opt.* **1**, 33 (1962).
- [2] T. Tajima and J. M. Dawson *Phys. Rev. Lett.* **43**, 267 (1979); <https://doi.org/10.1103/PhysRevLett.43.267>
- [3] Marlan O. Scully and M. S. Zubairy *Phys. Rev. A* **44**, 2656 (1991); <https://doi.org/10.1103/PhysRevA.44.2656>
- [4] E. S. Sarachik and G. T. Schappert, *Phys. Rev. D* **10**, 2738 (1970).
- [5] G. Malka, E. Lefebvre, and J. L. Miquel *Phys. Rev. Lett.* **78** (1997), 3314; <https://doi.org/10.1103/PhysRevLett.78.3314>
- [6] C. I. Moore, J. P. Knauer, and D. D. Meyerhofer, *Phys. Rev. Lett* **74**, 2439 (1995).
- [7] W. P. Leemans, B. Nagler, A. J. Gonsalves, Cs. Tth, K. Nakamura, C. G. R. Geddes, E. Esarey, C. B. Schroeder and S. M. Hooker *Nat. Phys.* **2**, 696 (2006).
- [8] W. P. Leemans et al., *Phys. Rev. Lett.* **113**, 245002; <https://doi.org/10.1103/PhysRevLett.113.245002>
- [9] A. Pukhov, Z.-M. Sheng, and J. Meyer-ter-Vehn, *Phys. Plasmas* **6**, 2847 (1999); <https://doi.org/10.1063/1.873242>
- [10] Gerard A. Mourou, Toshiki Tajima, and Sergei V. Bulanov *Rev. Mod. Phys.* **78**, 309 (2006); <https://doi.org/10.1103/RevModPhys.78.309>
- [11] E. Esarey, C. B. Schroeder, and W. P. Leemans *Rev. Mod. Phys.* **81**, 1229 (2009); <https://doi.org/10.1103/RevModPhys.81.1229>
- [12] Alexey V. Arefiev, Boris N. Breizman, Marius Schollmeier, and Vladimir N. Khudik *Phys. Rev. Lett.* **108**, 145004 (2012); <https://doi.org/10.1103/PhysRevLett.108.145004>
- [13] A. V. Arefiev, V. N. Khudik, A. P. L. Robinson, G. Shvets, L. Willingale, and M. Schollmeier *Phys. Plasmas* **23**, 056704 (2016); <https://doi.org/10.1063/1.4946024>
- [14] Tianhong Wang, Vladimir Khudik, Alexey Arefiev, and Gennady Shvets *Phys. Plasmas* **26**, 083101 (2019); <https://doi.org/10.1063/1.5110407>
- [15] K. A. Tanaka, K. M. Spohr, D. L. Balabanski, S. Balasubramanian, L. Capponi, M. O. Cernaianu, M. Cucuic, A. Cucoanes, I. Dancus, A. Dhal, B. Diaconescu, D. Doria, P. Ghenuche, D. G. Ghita, S. Kisiov, V. Nastasa, J. F. Ong, F. Rotaru, D. Sangwan, P.-A. Sderström, D. Stutman, G. Suliman, O. Tesileanu, L. Tudor, N. Tsoneva, C. A. Ur, D. Ursescu, and N. V. Zamfir *Matter and Radiation at Extremes* **5**, 024402 (2020); <https://doi.org/10.1063/1.5093535>
- [16] Feng He, Wei Yu, Peixiang Lu, Han Xu, Liejia Qian, Baifei Shen, Xiao Yuan, Ruxin Li and Zhizhan Xu, *Phys. Rev. E* **68**, 046407 (2003).
- [17] He Feng, Yu Wei, Lu Peixiang and Xu Han *Plasma Sci. Technolgy* **6** 2492 (2004); <http://iopscience.iop.org/1009-0630/6/5/013>
- [18] M. Kalashnikov, A. Andreev, K. Ivanov, A. Galkin, V. Korobkin, M. Romanovsky, O. Shiryaev, M. Schnuerer, J. Braenzel, V. Trofimov *Laser and Particle Beams*, **33**(3), 361-366 (2015); doi:10.1017/S0263034615000403
- [19] E. Esarey, P. Sprangle and J. Krall, *Phys. Rev. E* **52**, 5443 (1995).
- [20] F. V. Hartemann, S. N. Fochs, G. P. Le Sage, N. C. Luhmann, Jr., J. G. Woodworth, M. D. Perry, Y. J. Chen and A. K. Kerman, *Phys. Rev. E* **51**, 4833 (1995).
- [21] F. V. Hartemann, J. R. Van Meter, A. L. Troha, E. C. Landahl, N. C. Luhmann, Jr., J. G. Woodworth, H. A. Baldis, Atul. Gupta and A. K. Kerman, *Phys. Rev. E* **58**, 5001 (1998).
- [22] B. Quesnel and P. Mora, *Phys. Rev. E* **58**, 3791 (1998).
- [23] G. V. Stupakov and M. S. Zolotarev, *Phys. Rev. Lett* **86**, 5274 (2000).
- [24] P. X. Wang, Y. K. Ho, X. Q. Yuan, Q. Kong, N. Cao, L. Shao, A. M. Sessler, E. Esarey, E. Moshkovich, Y. Nishida, N. Yugami, H. Ito, J. X. Wang, and S. Scheid *Journal of Applied Physics* **91**, 856 (2002); <https://doi.org/10.1063/1.1423394>
- [25] A. Maltsev and T. Ditmire *Phys. Rev. Lett.* **90**, 053002 (2002); <https://doi.org/10.1103/PhysRevLett.90.053002>
- [26] Yousef I. Salamin and Christoph H. Keitel *Phys. Rev. Lett.* **88**, 095005; <https://doi.org/10.1103/PhysRevLett.88.095005>
- [27] I. Y. Dodin and N. J. Fisch *Phys. Rev. E* **68**, 056402 (2003); <https://doi.org/10.1103/PhysRevE.68.056402>
- [28] He Feng, Yu Wei, Lu Peixiang, Xu Han, Shen Baifei, Li Ruxin and Xu Zhizhan, *Plasma Science and Technology*, Vol.7, No. 4, 2968 (2005).
- [29] Yousef I. Salamin *Phys. Rev. A* **73**, 043402 (2006); <https://doi.org/10.1103/PhysRevA.73.043402>
- [30] Devki Nandan Gupta, Niti Kant, Dong Eon Kim, and Hyyong Suk *Phys. Lett. A* **368** (2007) 402407; <https://doi.org/10.1016/j.physleta.2007.04.030>

- [31] A. L. Galkin, V. V. Korobkin, M. Yu. Romanovsky, and O. B. Shiryayev Phys. Plasmas 15, 023104 (2008); <https://doi.org/10.1063/1.2839349>
- [32] Yousef I. Salamin, Zoltán Harman, and Christoph H. Keitel Phys. Rev. Lett. **100**, 155004 (2008); <https://doi.org/10.1103/PhysRevLett.100.155004>
- [33] Zoltán Harman, Yousef I. Salamin, Benjamin J. Galow, and Christoph H. Keitel Phys. Rev. A 84, 053814 (2011); <https://doi.org/10.1103/PhysRevA.84.053814>
- [34] Pierre-Louis Fortin, Michel Pieche and Charles Varin, J. Phys. B: At. Mol. Opt **43**, 025401 (2010).
- [35] A. P. L. Robinson, A. V. Arefiev, and D. Neely Phys. Rev. Lett. **111**, 065002 (2013); <https://doi.org/10.1103/PhysRevLett.111.065002>
- [36] Harjit Singh Ghotra and Niti Kant Optics Communications 383 (2017) 169176; <https://doi.org/10.1016/j.optcom.2016.08.061>
- [37] Niti Kant, Jyoti Rajput and Arvinder Singh Eur. Phys. J. D 74: 142 (2020); <https://doi.org/10.1140/epjd/e2020-100241-y>
- [38] J. D. Jackson, *Classical Electrodynamics*, Third Edition, John Wiley & Sons, New York, (1999).
- [39] A. E. Siegman, *Lasers*, University Science Books; Revised ed. edition (1986).
- [40] P. F. Goldsmith, *Quasioptical Systems: Gaussian Beam Quasioptical Propagation and Applications* Wiley-IEEE Press (1998).
- [41] Y. Y. Li, Y. J. Gu, Z. Zhu, X. F. Li, H. Y. Ban, Q. Kong, and S. Kawata Phys. Plasmas 18, 053104 (2011); <https://doi.org/10.1063/1.3581062>
- [42] Lorenzo Cicchitelli, H. Hora, and R. Postle Phys. Rev. A 41, 3727 (1990); <https://doi.org/10.1103/PhysRevA.41.3727>
- [43] M. Rezaei-Pandari, M. Akhyani, F. Jahangiri, A.R. Niknam, R. Massudi Optics Communications 429 (2018) 4652; <https://doi.org/10.1016/j.optcom.2018.07.081>
- [44] Thévenet, M., Leblanc, A., Kahaly, S. et al. Nature Phys 12, 355360 (2016); <https://doi.org/10.1038/nphys3597>
- [45] Meng Wen, Yousef I. Salamin, and Christoph H. Keitel Phys. Rev. Applied 13, 034001; <https://doi.org/10.1103/PhysRevApplied.13.034001>